

Theory of Multifrequency Atomic Force Microscopy

Jose R. Lozano and Ricardo Garcia*

Instituto de Microelectrónica de Madrid, CSIC, Isaac Newton 8, 28760 Tres Cantos, Madrid, Spain

(Received 17 October 2007; published 20 February 2008)

We develop a theory that explains the origin of the high force sensitivity observed in multifrequency force microscopy experiments. The ability of the microscope to extract complementary information on the surface properties is increased by the simultaneous excitation of several flexural cantilever modes. The force sensitivity in multifrequency operation is about 0.2 pN. The analytical model identifies the virial and the energy dissipated by the tip-surface forces as the parameters responsible for the material contrast. The agreement obtained among the theory, experiments and numerical simulations validates the model.

DOI: [10.1103/PhysRevLett.100.076102](https://doi.org/10.1103/PhysRevLett.100.076102)

PACS numbers: 68.37.Ps, 07.79.Lh, 62.25.-g, 62.30.+d

Progress on spatial resolution and compositional sensitivity is one of the dominant driving forces that both stimulates and shapes the evolution of force microscopy methods (AFM). The technique has evolved from monitoring the static deflection of the cantilever to the dynamic excitation and detection of the cantilever-tip oscillation [1–6]. The need for higher compositional resolution and sensitivity at the molecular level has led to explore AFM imaging with higher harmonics as well as with other flexural or torsional cantilever modes [7–19]. More recently, the AFM is experiencing the evolution from single to multifrequency excitation and detection schemes of the cantilever-tip motion [20–28].

Multifrequency AFM has shown a remarkable enhancement of sensitivity of the microscope to image in a gentle manner and with high spatial resolution a variety of heterogeneous materials. Compositional maps of conjugated molecular materials show a contrast that is about 1 order of magnitude higher than the one achieved in amplitude modulation AFM (the most popular among the various dynamic AFM modes) [22]. Proksch has shown that dual-frequency excitation produces maps of the surface of graphite that can be related to its electronic properties [21]. Stark *et al.* have used this method to minimize the cross talk between mechanical and electrical interactions while imaging charge patterns in electrets [23]. The sensitivity of multifrequency AFM has been exploited to measure subnanometer displacements in microelectromechanical devices [25]. Maximum tip-molecule forces of 35 pN have been reported while imaging antibodies [27]. In liquids, Basak and Raman have shown that the second flexural mode is excited by the tip-surface interactions [28]. Multifrequency excitation has also been reported to control nonlinear dynamics effects in force microscopy imaging [26].

In multifrequency AFM the cantilever-tip ensemble is simultaneously excited by several driving forces [22]. Usually the excitation signal involves two different driving forces (bimodal operation), although excitation over a band of frequencies has also been reported [24]. Our study will

be focused on studying bimodal-frequency excitation experiments. The excitation frequencies are tuned to match two of the flexural modes of the cantilever, usually the first and second resonances. The output signal of the amplitude of the first mode is used to image the topography of the surface, similarly to tapping mode AFM. An output signal of the second mode, usually the phase shift, is used to map changes in mechanical, magnetic or electrical properties of the surface. The technique offers a straightforward approach to separate topography from other interactions influencing the tip motion. Thus the different modes act as signal channels that separate the sample properties. The technique, on the other hand, can be easily implemented in existing AFMs.

The rationale for using AFM schemes based on the simultaneous excitation of several higher modes relies on numerical simulations [11]. It has also been loosely formulated in terms of the higher quality factor, optical sensitivity and force constant of the higher modes [27]. However, none of the above factors nor their combination explains the observed contrast.

In this letter we develop a theory of bimodal-frequency AFM imaging that identifies both the virial of the conservative tip-surface forces and energy dissipation processes as the parameters that carry information on the coupling of the excited modes. The second excitation enhances the coupling between modes, which in turns, enables to increase the force sensitivity to mechanical, magnetic or electric interactions of the microscope. In contrast with regular AM-AFM operation, the material contrast persists even in the absence of energy dissipation processes. Furthermore, the theory also shows that any representation of the phase shift of one mode with respect to the other can be used to enhance the sensitivity of the instrument. The quantitative agreement obtained among theory, numerical simulations and experiments performed on mica samples supports the theory.

To describe the dynamics of the cantilever-tip system in force microscopy we model the cantilever as a rectangular beam [8,14,27]. To develop analytical expressions, the

Euler-Bernoulli partial differential equation of the AFM is approached by a system of n second order differential equations, one for each eigenmode of the cantilever. We also assume that dynamics of the system is mostly contained in the lower eigenmodes. Then we obtain a system of two differential equations,

$$m\ddot{z}_1 = -k_1 z_1 - \frac{m\omega_1}{Q_1} \dot{z}_1 + F_1 \cos\omega_1 t + F_2 \cos\omega_2 t + F_{ts}(z_1 + z_2), \quad (1)$$

$$m\ddot{z}_2 = -k_2 z_2 - \frac{m\omega_2}{Q_2} \dot{z}_2 + F_1 \cos\omega_1 t + F_2 \cos\omega_2 t + F_{ts}(z_1 + z_2), \quad (2)$$

where m is the effective mass of the cantilever; Q_i , k_i , A_{0i} , F_i , and $\omega_i = 2\pi f_i$ are, respectively, the quality factor, force constant, free amplitude, external excitation force ($F_i = k_i A_{0i}/Q_i$), and angular frequency of the i eigenmode. The solution of the above system can be approached by,

$$z(t) = z_1(t) + z_2(t) + O(\varepsilon) \approx A_1 \cos(\omega_1 t - \phi_1) + A_2 \cos(\omega_2 t - \phi_2), \quad (3)$$

where A_i is the amplitude and ϕ_i is the phase shift of the $-i-$ eigenmode; $O(\varepsilon)$ is a term that carries the contribution of the other modes and harmonics.

The virial theorem and energy-conservation principles can be used to derive analytical relationships in dynamic AFM [29–31]. In this system the virial of the tip-surface interaction can be decomposed in the eigemode virials,

$$V_{ts} = \frac{1}{T} \int_0^T F_{ts}(t) z(t) dt = V_{ts}(1) + V_{ts}(2), \quad (4)$$

where the virial is expressed as the sum of the tip-surface eigemode virials.

$$V_{ts}(i) = \frac{1}{T} \int_0^T F_{ts}(t) z_i(t) dt = -\frac{1}{2} F_i A_i \cos\phi_i. \quad (5)$$

When there is not dissipation on the sample surface ($E_{ts} = 0$), the virial of the interaction can also be expressed as,

$$V_{ts} = \frac{1}{2} \left[F_1 A_1 \sqrt{1 - \left(\frac{A_1}{A_{01}}\right)^2} - F_2 A_{02} \sin\phi_2 \cos\phi_2 \right]. \quad (6)$$

In the above equations we have not included the contribution from the static deflection of the cantilever. Manipulation of Eqs. (1) to (5) leads to the following result [32]

$$\phi_i = -\arctan\left(\frac{1 \pm \sqrt{1 - (4\nu_i)^2 - 4\beta_i}}{4\nu_i}\right), \quad (7)$$

where $\nu_i = Q_i V_{ts}(i)/(k_i A_{0i}^2)$ and $\beta_i = Q_i E_{ts}(i)/(\pi k_i A_{0i}^2)$. β_i is proportional to the energy dissipated per cycle by the mode i on the surface. The virial term carries

information on conservative processes. It can be shown that the virial of velocity dependent forces is zero.

Equation (7) links observables such as ϕ_i with conservative ($V_{ts}(i)$) and nonconservative interactions ($E_{ts}(i)$). At this point we would like to emphasize that the above expressions are valid for any kind of tip-surface interaction as long as Eq. (3) remains a good approximation.

To compare theory, simulations and experiments at very low forces, we focus on long-range attractive tip-surface interactions given by $F_{ts} = -[HR/6d^2]$ where H is the Hamaker constant, R the tip radius and d the instantaneous tip-surface distance. We consider a cantilever that has a length L , width b and thickness h of 225 μm , 40 μm , 1.8 μm respectively; its Young's modulus E and mass density ρ are 170 GPa and 2320 kg/m^3 respectively. The force constants, resonance frequencies and quality factors of modes 1 and 2 are 0.9 N/m, 35.2 N/m, $f_1 = 48.913$ kHz, $f_2 = 306.194$ kHz, 255 and 1000, respectively. The tip radius R is 20 nm. To solve the Euler-Bernoulli equation we have followed the protocol described in Refs. [11,27].

The dependence of the amplitude on the average tip-surface distance for single (conventional case) and bimodal frequency excitation are shown in Fig. 1. For single excitations (monomodal hereafter), the amplitude decreases from its free value either $A_{01} = 10$ nm or $A_{02} = 1$ nm rather linearly with the distance. The amplitude of both modes under monomodal excitation shows a similar be-

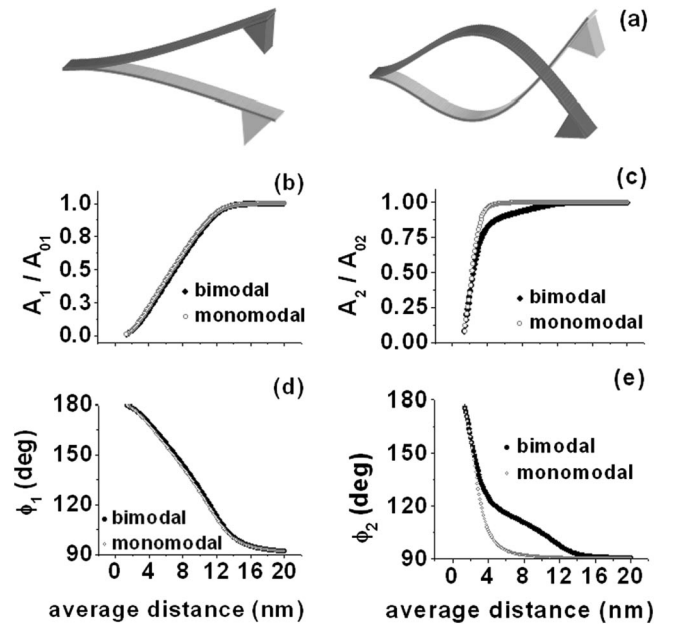


FIG. 1. (a) Cantilever geometries of the first (left) and second flexural modes (right). (b) First mode amplitude curve for monomodal (open dots) and bimodal-frequency excitations (dark dots). (c) Second mode amplitude curve for monomodal (open dots) and bimodal (dark dots) excitations. (d) First mode and (e) second mode phase shifts. $A_{01} = 10$ nm, $A_{02} = 1$ nm; $H = 9.03 \times 10^{-20}$ J. See cantilever description in the main text for the other parameters. The same applies for Figs. 2–4.

havior. Figure 1(b) shows that the amplitude of the first mode is almost independent on the excitation method (monomodal vs. bimodal). This is a consequence of the amplitude ratio used here $A_{02}/A_{01} = 0.1$. More importantly, it indicates that under bimodal excitation, the amplitude of the first mode can be used as a feedback parameter to track the topography. On the other hand, the amplitude of the second mode shows a marked dependence on the excitation mode [Fig. 1(c)]. Similar conclusions can be drawn for the respective phase shifts [Fig. 1(d) and 1(e)]. Under bimodal excitation, the second mode probes the tip-surface interactions at larger tip-surface average distances. This property explains the ability of the AFM under bimodal excitation instrument to acquire images by applying maximum forces below 100 pN. The force sensitivity under bimodal excitation can be estimated by calculating the smallest force change that produces a phase shift variation above the noise level ($\varphi_i \sim 0.05\text{--}0.1^\circ$). In this way we obtain a value of 0.2 pN.

Figure 2 shows the time dependence of the tip deflection under bimodal excitation in the absence of tip-surface forces (free case) ($A_{01} = 6$ nm, $A_{02} = 1$ nm). The fast Fourier transform (FFT) of the oscillation shows two peaks corresponding to the first two eigenmodes of the cantilever [Fig. 2(b)]. In the presence of tip-surface interaction forces, the nonlinear forces introduce higher order harmonics that distort the oscillation. In Fig. 2(c) the tip has been approached to reach an amplitude of $A_1 = 4.4$ nm. Besides the above peaks we also observe several minor peaks [Fig. 2(d)]. We found that the frequency of those peaks can be expressed as $mf_1 + nf_2$, where f_i is the flexural frequency of mode i and m and n are integer numbers. Nonetheless, the amplitude of those peaks is below the noise level in AFM ($\sim 10^{-2}$ nm). The comparison between

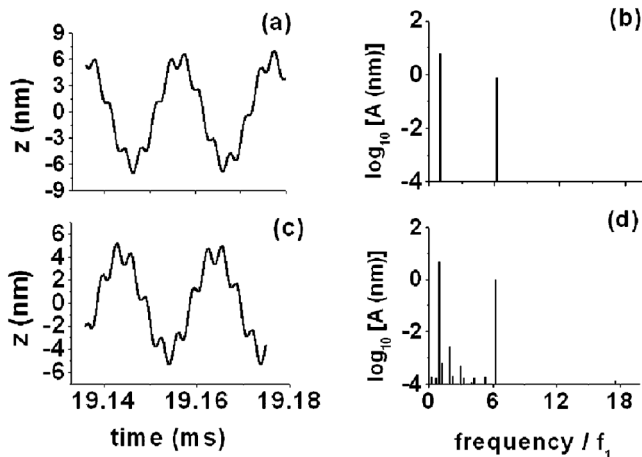


FIG. 2. (a) Time dependence of the tip deflection under bimodal-frequency excitation in the absence of tip-surface forces. (b) FFT of the wave form shown in (a). (c) Time dependence of the tip deflection under bimodal-frequency excitation for a tip that interacts with a surface, $A_1 = 4.4$ nm. (d) FFT of the signal shown in (c) $A_{01} = 6$ nm, $A_{02} = 1$ nm, $H = 9.03 \times 10^{-20}$ J.

Figs. 2(a) and 2(b) with 2(c) and 2(d) shows that the amplitude ratio A_2/A_1 increases by reducing the set-point amplitude. This is explained by comparing the slopes of the two flexural modes under bimodal excitation $dA_1/dz \geq dA_2/dz$ in the 4 to 12 nm range [Figs. 1(b) and 1(c)].

The validity of Eq. (7) is demonstrated by comparing its results with numerical simulations of the adapted Euler-Bernoulli differential equation for AFM [Fig. 3(a)] and with experimental results performed on a mica surface [Fig. 3(b)]. In both cases there is a good quantitative agreement. The curves are determined by recording the phase shift and amplitude signals while the tip is approached towards the sample surface. In the calculations we have used two different Hamaker constants, $H = 1 \times 10^{-20}$ and $H = 9.03 \times 10^{-20}$ J. The latter corresponds to the interaction of a silicon dioxide tip with a mica surface. The shape of the curves do show a noticeable dependence on the strength of the interaction, however, the analytical expression does reproduce both cases.

Figure 4 emphasizes the importance of using crossed plots to achieve material contrast, and at the same time, it establishes that the observed contrast is an intrinsic property of multifrequency AFM. Figures 4(a) and 4(b) show the dependence of the virial of the first mode under bimodal excitation with respect to the modal amplitudes. The virial data is easily transformed into the experimental observable (φ_i) by using Eq. (7) (here $\beta_i = 0$). The curves overlap when the virial 1 is plotted against its amplitude. On the other hand, material contrast is obtained when the representation involves the amplitude of the second mode. Identical results are obtained when the virial of the second mode is plotted with respect to the modal amplitudes [Figs. 4(c) and 4(d)]. This result is analytically expressed in Eq. (6), where the variables of the different modes are coupled through the total virial of the system. We conclude that material contrast is readily obtained when the virial of one mode is plotted versus the amplitude of the other. The materials simulated have $H = 9.03 \times 10^{-20}$ J and 4.7×10^{-20} J. They correspond, respectively, to the interaction

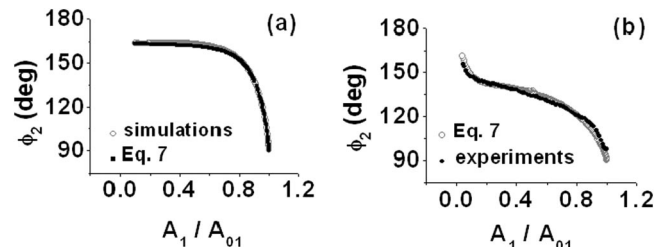


FIG. 3. Dependence of the second mode phase shift with respect to the amplitude of the first mode as given by numerical simulations, analytical model and experiments. (a) Comparison between the numerical solution and the analytical expression [Eq. (7)]; $H = 1 \times 10^{-20}$ J. (b) Comparison between theory and experimental measurements on mica $H = 9.03 \times 10^{-20}$ J (adapted from Ref. [27]) and results given by the analytical equation.

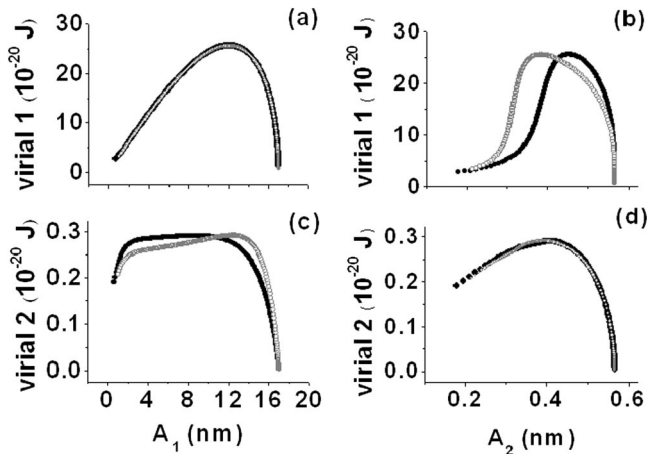


FIG. 4. Dependence of the virial for two different materials, open dots $H = 4.7 \times 10^{-20}$ J, dark dots $H = 9.03 \times 10^{-20}$ J. (a) First mode virial with respect to the first mode amplitude. (b) First mode virial with respect to the second mode amplitude. (c) Second mode virial with respect to the first mode amplitude. (d) Second mode virial with respect to the second mode amplitude.

of a silicon dioxide tip with a mica surface and, with a surface formed by a few monolayers of water adsorbed on mica [33].

The analytical expressions together with numerical simulations allow us to propose an explanation for the enhanced sensitivity provided by multifrequency AFM. Under bimodal-frequency excitation, the different eigenmodes of the microcantilever are coupled by the virial of the tip-surface forces. Then, the second mode can probe the tip-surface forces in a way that is not hindered by the feedback mechanism as it happens in conventional amplitude modulation AFM. The simultaneous excitation enables the microscope to increase its information channels from two to four. The consequence of this approach is twofold. First, it enables to probe the material properties at larger distances and thus in turn to enhance the sensitivity. Second, material contrast could be obtained for exclusively conservative interactions. This in turns suppress or minimizes surface damage.

This work was financially supported by the European Commission (FORCETOOL, No. NMP4-CT-2004-013684), Ministerio de Educación y Ciencia (No. MAT2006-03833). We do thank stimulating discussions with N. F. Martínez and S. Patil.

*rgarcia@imm.cnm.csic.es

- [1] G. Binnig, C. F. Quate, and C. Gerber, *Phys. Rev. Lett.* **56**, 930 (1986).
- [2] F. J. Giessibl and C. F. Quate, *Phys. Today* **59**, No. 12, 44 (2006).
- [3] E. Meyer, H. J. Hug, and R. Bennewitz, *Scanning Probe Microscopy: Lab on a Tip* (Springer-Verlag, Berlin, 2004).

- [4] J. K. H. Hörber and M. J. Miles, *Science* **302**, 1002 (2003).
- [5] C. Bustamante and D. Keller, *Phys. Today* **48**, No. 12, 32 (1995).
- [6] D. Rugar and P. Hansma, *Phys. Today* **43**, No. 10, 23 (1990).
- [7] S. C. Minne, S. R. Manalis, A. Atalar, and C. F. Quate, *Appl. Phys. Lett.* **68**, 1427 (1996).
- [8] R. W. Stark and W. M. Heckl, *Surf. Sci.* **457**, 219 (2000).
- [9] M. Stark, R. W. Stark, W. Heckl, and R. Guckenberger, *Appl. Phys. Lett.* **77**, 3293 (2000).
- [10] O. Sahin, C. F. Quate, O. Sogaard, and A. Atalar, *Phys. Rev. B* **69**, 165416 (2004).
- [11] T. R. Rodriguez and R. Garcia, *Appl. Phys. Lett.* **84**, 449 (2004).
- [12] S. Crittenden, A. Raman, and R. Reifenger, *Phys. Rev. B* **72**, 235422 (2005).
- [13] R. Gabai, L. Segev, and E. Joselevich, *J. Am. Chem. Soc.* **127**, 11 390 (2005).
- [14] D. W. Dareing, T. Thundat, S. Jeon, and M. Nicholson, *J. Appl. Phys.* **97**, 084902 (2005).
- [15] J. Legleiter, M. Park, B. Cusik, and T. Kowalewski, *Proc. Natl. Acad. Sci. U.S.A.* **103**, 4813 (2006).
- [16] S. Sadewasser, G. Villanueva, and J. A. Plaza, *Appl. Phys. Lett.* **89**, 033106 (2006).
- [17] O. Sahin, S. Magonov, C. Su, C. F. Quate, and O. Solgaard, *Nature Nanotechnology* **2**, 507 (2007).
- [18] J. Preiner, J. Tang, V. Pastushenko, and P. Hinterdorfer, *Phys. Rev. Lett.* **99**, 046102 (2007).
- [19] Y. Sugimoto, S. Innami, M. Abe, O. Custance, and S. Morita, *Appl. Phys. Lett.* **91**, 093120 (2007).
- [20] FORCETOOL project, www.imm.cnm.csic.es/ForceTool.
- [21] R. Proksch, *Appl. Phys. Lett.* **89**, 113121 (2006).
- [22] N. F. Martínez, S. Patil, J. R. Lozano, and R. Garcia, *Appl. Phys. Lett.* **89**, 153115 (2006).
- [23] R. W. Stark, N. Naujoks, and A. Stemmer, *Nanotechnology* **18**, 065502 (2007).
- [24] S. Jesse, S. V. Kailin, R. Proksch, A. P. Baddorf, and B. J. Rodriguez, *Nanotechnology* **18**, 435503 (2007).
- [25] A. San Paulo, J. P. Black, R. M. White, and J. Bokor, *Appl. Phys. Lett.* **91**, 053116 (2007).
- [26] P. Thota, S. MacLaren, and H. Dankowicz, *Appl. Phys. Lett.* **91**, 093108 (2007).
- [27] S. Patil, N. F. Martínez, J. R. Lozano, and R. Garcia, *J. Mol. Recognit.* **20**, 516 (2007).
- [28] S. Basak and A. Raman, *Appl. Phys. Lett.* **91**, 064107 (2007).
- [29] A. San Paulo and R. Garcia, *Phys. Rev. B* **64**, 193411 (2001).
- [30] B. Anczykowski, B. Gotsman, H. Fuchs, J. P. Cleveland, and V. B. Elings, *Appl. Surf. Sci.* **140**, 376 (1999).
- [31] R. Garcia, C. J. Gomez, N. F. Martínez, S. Patil, C. Dietz, and R. Magerle, *Phys. Rev. Lett.* **97**, 016103 (2006); R. Garcia, R. Magerle, and R. Perez, *Nat. Mater.* **6**, 405 (2007).
- [32] See EPAPS Document No. E-PRLTAO-100-029808 for a complete description of the procedure to deduce the equations. For more information on EPAPS, see <http://www.aip.org/pubservs/epaps.html>.
- [33] J. Israelachvili, *Intermolecular and Surface Forces* (Academic, London, 1994), 2nd ed.